

## Spatial Analysis of Tropical Cyclone Yaas using Satellite Data

N. Umakanth<sup>1a</sup>, Rajesh Gogineni<sup>2b</sup>, K. Madan Mohan Rao<sup>3c</sup>, B. Revanth Reddy<sup>4c</sup>, Sk. Hasane Ahammad<sup>5d</sup> and M.C. Rao<sup>6e</sup>

**Abstract:** Tropical cyclones are the major natural disasters in India. They cause high death toll and property destruction, that lead to a negative socioeconomic impact. For early warning alerts, real-time monitoring, impact and damage pre-assessment, and relief operations, remote sensing and geographic information systems (GIS) are helpful. Tropical cyclone warning bulletins detail the cyclone intensity, direction and position of occurrence of cyclonic event, velocity of the winds across the coastal areas, expected landfall site. During the period of May 23<sup>rd</sup> to May 28<sup>th</sup>, 2021, an attempt was made to examine Yaas cyclone over Bay of Bengal Sea (BOBS). Rainfall (RF), Convective available potential energy (CAPE), cloud top temperature (CTT), total precipitable water (TPW), lifted index (LI), convective inhibition (CIN), sea level pressure (SLP), divergence and sea surface temperature (SST) are used to analyze cyclonic activity. Cold dry air from high latitudes meet with warm moist air in low latitudes leading to instability. This instability is responsible for the conducive feature in convection occurrence. The weather research forecasting (WRF) model forecast results matched well with MERRA2 reanalysis results. The model performed well in prior occurrence of convection activity.

**Keywords:** Convective inhibition, sea level pressure, cloud top temperature, sea surface temperature.

### 1. Introduction

Tropical cyclones originating in the Indian Ocean pose the greatest threat to countries in South Asia, particularly those located near the Bay of Bengal (BOBS). More than 80% of major cyclonic activities took place in BOBS of North Indian Ocean. In the BOBS, 5–6 tropical cyclones form each year, with roughly two of them becoming severe. The majority of BOBS severe cyclones form in the post-monsoon season, between October and November. In May month, high intensity cyclones were observed but the most damaging cyclonic activities were observed in post-monsoon season. We usually observe high formation of low pressure systems during post-monsoon season over South Asia (Singh, 2007). Most cyclones formed in BOBS made their landfall on Bangladesh's coast since the BOBS funnel shape terminates here.

In cyclone-prone areas, the influence of powerful winds, torrential rains and storm surges (abnormally high sea levels) are seen that lead to high death rate and damage to public life. Winds

over 117 kilometers per hour often damage delicate structures (Hossain & Mullick, 2020). Heavy rain can cause catastrophic floods and considerable crop damage in a short period of time. In few occasions, nearly 50 cms of rainfall will be recorded in 3-7 days time period (Dasgupta et al. 2010). Several cyclones have blasted on the BOBS in the last 35 years, inflicting massive disruptions, damages and a staggering number of deaths (Hossain et al. 2008; Islam et al. 2011). Few are, in 1970 Bhola cyclone, in 1991 Hurricane, in 1997 BOB 07, in 2002 06B, in 2007 Sidr cyclone, in 2008 Rashmi cyclone, in 2009 Aila cyclone, in 2013 Mahasen cyclone, in 2015 Komen cyclone, in 2016 Rohanu cyclone, in 2017 Mora cyclone and in 2019 Fani cyclone. The 1970 Bhola cyclone was a powerful hurricane that hit India on November 12<sup>th</sup>, 1970, killing an estimated 250,000 people and making it one of the deadliest natural catastrophes in modern history (Islam & Peterson, 2009). In 1985, Urir Char and Sandwip cyclones occurred and they were researched to understand the factors that contributed to high cyclone related fatality rates. In Sandwip cyclone, eight cyclone shelters were arranged whereas in Urir Char cyclone, 40% of people along the cyclone hit area were dead due to lack of cyclone shelters (Siddique & Eusof, 1987). On April 29<sup>th</sup>, 1991, at 19:00 UTC, a hurricane hit the Chittagong shoreline, located northeast of the BOBS, with winds of 240 km/h, killing approximately one and half lakh people over Bangladesh region (Chowdhury et al. 1993). The people most vulnerable to cyclones around the coastal places are those with little economic resources, outmoded technology, poor knowledge on cyclones mitigation aspects and poor infrastructure. Such communities are failing to execute perfect rescue plans to defend the people against the cyclones (O'Hare, 2001). As a result of climate change,

#### Authors information:

<sup>a</sup>Indian Institute of Tropical Meteorology (IITM), Dr. Homi Bhabha Road, Pashan, Pune, Maharashtra 411008, INDIA. E-mail: numakanth23@gmail.com<sup>1</sup>

<sup>b</sup>Department of ECE, Dhanekula Institute of Engineering and Technology, Vijayawada-521139, INDIA. E-mail: rgogineni9@gmail.com<sup>2</sup>

<sup>c</sup>Indian Institute of Tropical Meteorology (IITM), Dr. Homi Bhabha Road, Pashan, Pune, Maharashtra 411008, INDIA. E-mail: kmadan.rao@tropmet.res.in<sup>3</sup>; revanthreddy93.b@gmail.com<sup>4</sup>

<sup>d</sup>Department of ECE, Koneru Lakshmaiah Education Foundation, Vaddeswaram-522502, INDIA. E-mail: ahammadklu@gmail.com<sup>5</sup>

<sup>e</sup>Department of Physics, Andhra Loyola College, Vijayawada-520008, INDIA. E-mail: raomc72@gmail.com<sup>6</sup>

\*Corresponding Author: raomc72@gmail.com

Received: June 12, 2023

Accepted: January 18, 2024

Published: December 31, 2024

cyclonic events may occur at any time (Karim & Mimura, 2008).

The cyclones that pass through BOBS have both beneficial and harmful consequences. From a meteorological standpoint, these cyclones are linked to a lot of rain and these rains affect the hydrological cycle with raising groundwater levels by filling rivers that increase the water flows at dams. Despite recent advances in weather prediction, predicting cyclone intensity is still challenging. For a better prediction, it is also essential to comprehend the characteristics of cyclogenesis and the mechanisms that lead to their intensification over BOBS (Webster, 2008; McPhaden et al. 2009; Wu et al. 2012; Sreenivas et al. 2012a; Sreenivas et al. 2012b; Sreenivas and Gnanaseelan 2014; DeMaria, 1996; Balaguru et al. 2012; Zehr 2003).

A week after Cyclone Tauktae wreaked devastation on India's west coast, Cyclone Yaas made landfall in Odisha and West Bengal on the east coast, leaving a trail of death and destruction in its wake. India is the sixth-most severely impacted nation in the world in 2019 according to the Global Climate Risk Index 2021. The main obstacles for researchers studying tropical cyclogenesis include a lack of information about large tropical basins, a lack of data on tropical cyclone formation despite the existence of long-term large-scale conditions that favor cyclone occurrence, variations in atmospheric patterns, and ocean currents of various ocean basins (Mazzarella et al. 2014). Investigations are still ongoing to understand the crucial factors that affect whether cloud clusters develop into tropical storms. Karyampudi and Pierce (2002) looked into how different mesoscale elements interacted during the early stages of tropical storm formation. Venkatesh (2006) noted the mesoscale interaction that took place during the development and intensification of the 1999 superstorm in Orissa. In order to distinguish between developing and non-developing cloud clusters, Mazzarella et al. (2014) employed lightning data as a proxy for convective activity. According to descriptions by Zehnder and Gall (1991) and Velasco and Fritsch (1987), tropical Storm Priscilla began life as a mesoscale convective system (MSCSM) over a land area in 1989. Hurricane season was established in 1989 because of the increased number of hurricanes that year. Prior to the development of the MSCSM, the influence of moisture and vertical wind profiles during that season set the path for cyclone formation (Smith and Gall, 1989; Siewert et al. 2010, König, 2002).

In operational meteorology, the so-called instability indices are often used to identify the optimal conditions for the development of deep wet convection and severe weather. They are computed using profiles of atmospheric temperature and humidity. Thanks to the arrival of meteorological satellites, atmospheric instability is operationally determined using data that is worldwide and frequent (5–15 minutes). Compared to traditional radio-sounding metrics, the use of satellite data to develop instability indices results in significant gains in both temporal and spatial coverage (Purdum, 1976). As a result, Conte et al. (2011) looked into cyclones associated with various stability indices. They concluded

that the KI, LI, CAPE, and TPW variables significantly contribute to the establishment of deep convection. They also showed a direct relationship between indices and the frontal system of the storm. Since massive thunderstorms effectively encircle the cyclone's eye, the onset of the intense cyclonic rainfall is correlated with an increase in the CAPE value.

Furthermore, the region of thermodynamic disequilibrium that follows the route of the cyclone—that is, the warm, humid air at low altitudes and the cold, dry air at higher altitudes—is associated with the LI minimum. According to Conte et al. (2011), there is evidence of an impending explosive development of the cyclone due to the overlap of convection-friendly zones east of the Calabria region. This study provided us with the necessary motivation for this scientific endeavour. We have also investigated the relationship between these indicators and cyclones, drawing on the study work of Conte et al. (2011). Numerous research initiatives have centered on the creation of satellite-based sensors over the past 20 years (König and de Coning, 2009; Roberts and Rutledge, 2003; Seemann et al. 2003). The indices developed for the convective investigation based on satellite implementations are used in the current analysis. It is possible to track the progress of a cyclone using instability indicators. This was brought up by Moscatello et al. (2008) as yet another successful method for cyclone evolution. In a few instances, he examined the usefulness of such signs to the diagnosis of severe convection.

At the moment, the regular and thorough data gathered by geostationary satellite sensors, such as the onboard imager and sounder products, can be helpful for the quick identification of potentially severe weather characteristics. The most comprehensive depiction of historical weather and climate currently available is based on reanalysis data. They are based on a combination of recent short-term weather forecasts that have been revised and observations as well. The dynamical core, parameterizations and resolution of the reanalysis model all influence the output of severe events in reanalysis data. For example, newer generations of reanalyses produce better resolutions and use modern data assimilation methodologies. Many recent research, for example, have employed reanalysis data sets to construct tropical cyclone climatology, explore the impact of large-scale mechanisms on tropical storm evolution (Maloney & Hartmann, 2000; Maloney et al. 2000) and estimate tropical cyclone power dissipation (Srifer & Huber, 2006). As a result, greater representation of tropical cyclones in the reanalysis data set is critical for better understanding tropical storm inner core dynamics and interactions with the climate system (Scoccimarro et al. 2012). So, utilizing satellite data from May 23<sup>rd</sup> through May 28<sup>th</sup>, 2021, we tried to explore in this research the relationship between stability-related indicators and tropical cyclone Yaas over the Bay of Bengal Sea. The following is the paper's structure: The data and methodology utilized in the study are described in Section 2. Section 3 examines the findings and Section 4 summarizes the most important conclusions.

## 2. Data and Methodology

### Data

This study investigates the tropical cyclone Yaas. The Catastrophic Cyclone Yaas, which has a six-day duration (23<sup>rd</sup> to 28<sup>th</sup>, May 2021), first appeared in BOBS on May 23<sup>rd</sup> as a low-pressure system. By May 24<sup>th</sup>, the low pressure system had migrated westward and formed a deep depression. The storm quickly shifted north-eastward, steadily intensifying due to warm waters along the shore and the system was upgraded to a cyclonic storm and called Yaas later that day. Yaas intensified further on May 25<sup>th</sup>, becoming a severe cyclonic storm later that day. On May 26<sup>th</sup>, Yaas made a landfall near Odisha coast.

Global Precipitation Measurement (GPM) is a new generation of satellite precipitation products. Its objective is to develop the following-generation of a space measuring system that can perform routine and accurate measurements of global precipitation. The Tropical Rainfall Measuring Mission (TRMM) has been replaced by this. On the website <https://gpm.nasa.gov/data/directory> the GPM IMERG (Integrated Multi-satellite Retrievals for Global Precipitation Measurement) half-hourly rainfall data of 0.1°x0.1° have been downloaded (Huffman GJ et al., 2019). The most recent (5th generation) reanalysis data product from the European Centre for Medium-Range Weather Forecasts (ECMWF) has been put on a data server under the title of environmental services by the Copernicus Climate Change Service (C3S) (Hersbach et al., 2020). It is crucial to have access to these global data in order to comprehend the microphysical and dynamical aspects of earlier events. We used reanalysis data of the temperature and relative humidity in the study region with a spatial resolution of 0.250x0.250 for the current experiment. The data for the research region can be downloaded by users through the C3S data server (<https://cds.climate.copernicus.eu/cdsapp#!/home>). We computed the CAPE, CIN, TPW, and LI parameters using the temperature and relative humidity reanalysis data. All other parameters were taken from the MERRA2 dataset. Modern Era Retrospective Analysis for Research and Application (MERRA) data with a resolution of 0.25° was obtained from the website <https://disc.gsfc.nasa.gov/datasets?project=MERRA-2> from 23<sup>rd</sup> to 28<sup>th</sup> of May, 2021 (Gelaro et al. 2017). The FNL data has been downloaded from the website <https://rda.ucar.edu/datasets/ds083.2/>

### Methodology

The formulas used in this study's attempt to calculate the different indexes are listed below.

#### (i) Convective available potential energy (CAPE)

Moncrieff and Miller's (1976) formula is used to determine CAPE.

$$CAPE = \int_x^y g \left[ \frac{TV_{parcel} - TV_{env}}{TV_{env}} \right] dz \text{ ----- (1)}$$

Where  $TV_{parcel}$  represents the virtual temperature of an air parcel and  $TV_{env}$  represents the virtual temperature of an

environment respectively. The levels of free convection and neutral buoyancy are represented by x and y.

#### (ii) Lifted Index (LI)

This index is used to evaluate the troposphere's lowest levels. The LI threshold values are listed below (Galway, 1956).

$$\text{Lifted Index (LI)} = a_{500} - a_{parcel} \text{ ----- (2)}$$

Where a is the air temperature and  $a_{parcel}$  is the parcel temperature elevated from the ground to a pressure level of 500 hpa.

#### (iii) Total precipitable water (TPW)

In TPW, the amount of water vapour present in the air is expressed. The formula for calculating TPW is as follows:

$$TPW = \frac{1}{g} \int_{P_1}^{P_2} W dP \text{ ----- (3)}$$

Where  $P_1$  and  $P_2$  indicate the levels related to pressure, W denotes mixing ratio (Carlson TN et al.1990)

#### (iv) Convective Inhibition (CIN):

The Parker (2002) formula is used to calculate CIN.

$$CIN = \int_{Z_l}^{Z_f} g \left[ \frac{T_{v,parcel} - T_{v,env}}{T_{v,env}} \right] dz \text{ ----- (4)}$$

Where  $T_{v,parcel}$  indicates parcel's virtual temperature and  $T_{v,env}$  represents the environment's virtual temperature respectively.  $Z_f$  demonstrates the level of free convection and  $Z_l$  denotes the surface level.

#### (v) Storm Relative Helicity (SRLH):

The computation of SRLH is done to understand the updraft rotation of winds in cyclonic activity. This estimation is mainly done by considering the lower atmospheric level data such as from ground surface to one kilometer (Parker 2002).

SRLH is defined as

$$SRLH = \int_0^h \left( \frac{\vec{v}}{V} - \frac{\vec{c}}{C} \right) X \frac{d\vec{v}}{dz} dz \text{ ----- (5)}$$

Where V represents the environment's wind vector, C represents the storm's translation velocity,  $k \times dV/dz$  represents the horizontal vorticity and k represents the vertical unit vector, h is set to 3 kilometers in SCAN, as it is in other studies. The V(z) is the wind profile.

These metrics can indicate weather conditions that are conducive to the occurrence of severe weather if their values surpass specific thresholds, which are typically determined empirically and may change depending on the season and the location.

**Table 1.** Model Details

Model features	Specifications
Horizontal resolution	9 km
Vertical levels	42 levels
Radiation	RRTMG scheme
Cu_physics	Grell-Devenyi ensemble scheme
Planetary boundary layer	Yonsei University Scheme
Mp_physics	Morrison scheme
Surface layer physics	Revised MM5 Monin-Obukhov Scheme
Land surface physics	Noah Land Surface Model

### Weather Research Forecasting Model (WRF)

On May 26th, 2021, a cyclone associated with convection was predicted using WRF. For this study, the model is setup for 9Km resolution domain.

The WRF model is a next generation numerical weather prediction (NWP) model that is fully compressible and offers a range of features for enhanced comprehension of atmospheric processes and applications related to weather forecasting (Skamarock et al., 2019). The National Centre for Atmospheric Research (NCAR) in the United States developed it, and it was made available in 2000. Its scales vary from tens of meters to thousands of kilometres, making it suitable for a broad spectrum of meteorological applications. In WRF (version 3.9.1), the vertical momentum equation can be solved without the need for a hydrostatic approximation. Its two dynamical cores for solving the atmospheric governing equations are the Non-hydrostatic Mesoscale Model (NMM) and the Advanced Research WRF (ARW). Cloud-resolving simulations of the thunderclouds in this work are carried out using the ARW core. In order to improve the starting and boundary conditions, it offers a sophisticated data assimilation mechanism and strong multiple nesting capabilities.

A double-moment approach for the four hydrometeor classes—droplets, cloud ice, rain, and snow—is the Morrison scheme (Morrison et al., 2005). It is projected what the mass mixing ratios will be for five different types of hydrometeors: raindrops, pristine ice crystals, cloud liquid droplets, snow (big crystals or aggregates), and graupel or hail. Predictions are also made

regarding the overall concentrations of ice, snow, rain, and glaciers. Morrison approach considers new physically based parameterizations for simulating homogeneous and heterogeneous ice nucleation. A semi-analytic approach to the three phase (vapour, ice, and liquid) supersaturation equation is used to forecast the tendency rates of condensation/deposition and supersaturation field.

The National Center for Atmospheric Research (NCAR) created this model in collaboration with the National Center for Environmental Prediction (NCEP) of the National Oceanic and Atmospheric Administration (NOAA). We have utilized hybrid sigma vertical coordinate system. Following Rajeevan et al. (2010) for radiation schemes, the Rapid Radiative Transfer Model (RRTM) (Mlawer et al., 1997) was utilized for long wave radiation in all of the simulations, while the Dudhia short wave scheme (Dudhia, 1989) was employed for short wave radiation. The Rapid Radiative Transfer Model (RRTM) (Mlawer et al., 1997) long wave scheme is used to treat radiation in all simulations, which were inspired by Rajeevan et al. (2010). It takes into consideration various bands, trace gases, and species of microphysics. Short wave radiation has been addressed by the Dudhia Shortwave system (Dudhia, 1989). This short wave radiation strategy allows for clouds and clear-sky absorption and scattering due to its simple downward integration. Using the FNL (Final) Operational Global Analysis data from the NCEP, the model's fundamental initial conditions were gathered with a spatial resolution of 1 degree. The BOBS region employed in this study for WRF model prediction is situated between latitudes 0° and 30°N and longitudes 45° and 105°E. In this investigation, the 3.9.1 Model version was employed (Skamarock et al. 2008). Table 1 lists the model's most important characteristics. Thus, the WRF simulation began at 0000 UTC on May 22<sup>nd</sup> and ran for entire cyclonic event, while the storm made landfall at 0330 UTC on May 26<sup>th</sup>. The WRF model requires six hours to spin up. The model result displayed in this study was used for a 24-hour period, starting at 0000UTC on May 26<sup>th</sup>, 2021 and ending at 0000UTC on May 27<sup>th</sup>, 2021.

### 3.1 Results and discussion

Tropical cyclone Yaas travelled across the BOBS from May 23<sup>rd</sup> to May 28<sup>th</sup>, 2021 and this study looked into it. RF, CTT, CIN, SST, CAPE, SLP, LI, TPW and divergence are all used to assess cyclonic activity.

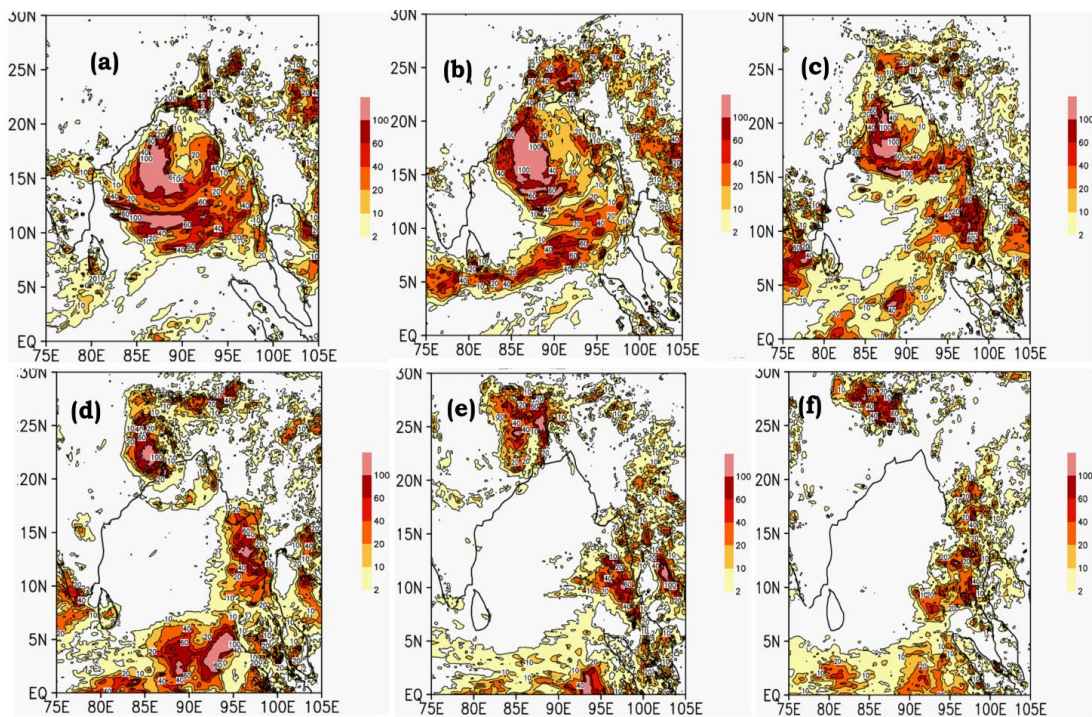


**Figure 1.** Spatial distribution of daily rainfall during (a) May 23<sup>rd</sup>, 2021, (b) May 24<sup>th</sup>, 2021, (c) May 25<sup>th</sup>, 2021, (d) May 26<sup>th</sup>, 2021, (e) May 27<sup>th</sup>, 2021, (f) May 28<sup>th</sup>, 2021.

We've drawn rainfall maps across the BOBS region in Figure 1 from May 23<sup>rd</sup> to May 28<sup>th</sup>, 2021. High rainfall is expected near the Northern Tamilnadu and Southern Andhra Pradesh coasts on May 23<sup>rd</sup>, 2021. The rainfall values range between 20 and 100 mm over BOBS (Figure 1 (a)). On 24<sup>th</sup> May, 2021, high rainfall is seen near Northern Andhra Pradesh and Southern Odisha coastal areas. The rainfall values range between 40 and 100 mm over BOBS (Figure 1 (b)). On 25<sup>th</sup> May, 2021, high rainfall is seen near Odisha coastal areas. The rainfall values range between 60 and 100 mm over BOBS (Figure 1 (c)). On 26<sup>th</sup> May, 2021, high rainfall is seen near Odisha coastal area Bahanaga. The rainfall values range between 60 and 100 mm over Dhamra port and Bahanaga area (Figure 1 (d)). On 27<sup>th</sup> May, 2021, the rainfall activity has been decreased near Odisha. The rainfall values range between 10 and 20 mm over BOBS (Figure 1 (e)). On 28<sup>th</sup> May, 2021, no rainfall is seen near Odisha and entire east coastal areas over BOBS (Figure 1 (f)).

We have plotted spatial maps of CTT over the BOBS region in Figure 2 from May 23<sup>rd</sup> to May 28<sup>th</sup>, 2021. On 23<sup>rd</sup> May, 2021 low CTT is seen near Northern Tamilnadu and Southern Andhra Pradesh coastal areas. The CTT values range between 180 and 200 K over BOBS (Figure 2(a)). On 24<sup>th</sup> May, 2021 low CTT is seen near Northern Andhra Pradesh coastal areas. The CTT values range between 180 and 200 K over BOBS (Figure 2(b)). On 25<sup>th</sup> May,

2021 low CTT is seen near Northern Andhra Pradesh coastal areas. The CTT values range between 180 and 190 K over BOBS (Figure 2(c)). On 26<sup>th</sup> May, 2021 very low CTT is seen near Odisha Coastal area Bahanaga. The CTT values range between 180 and 200 K over BOBS (Figure 2(d)). On 27<sup>th</sup> May, 2021 the CTT are higher near Odisha. The CTT values range between 200 and 210 K over BOBS (Figure 2(e)). On 28<sup>th</sup> May, 2021 the CTT values are seen increased near Odisha and Andhra Pradesh coastal areas over BOBS (Figure 2(f)). We have produced SST spatial maps across the BOBS region from May 23<sup>rd</sup> to May 28<sup>th</sup>, 2021 in Figure 3. SST readings in the BOBS region range from 30.5 to 31 degrees celsius on May 23<sup>rd</sup>, 2021 (Figure 3(a)). SST readings in the BOBS region on the 24<sup>th</sup> of May, 2021 vary from 30.3 to 31.2°C (Figure 3(b)). On 25<sup>th</sup> May, 2021, the high SST is seen near Northern Andhra Pradesh and Southern Odisha coastal areas. The SST values range between 29 and 30.9°C over BOBS (Figure 3(c)). On 26<sup>th</sup> May, 2021, high SST values are seen near Odisha coastal areas. Over BOBS, the SST values range from 30.5 to 31.10c (Figure 3(d)). The SST is comparatively lower near Odisha on May 27, 2021. Over BOBS, the SST values vary between 29.5 and 30°C (Figure 3(e)). The SST values are shown to be decreasing over BOBS on May 28, 2021, towards the coastal regions of Northern Andhra Pradesh and Southern Odisha (Figure 3(f)).

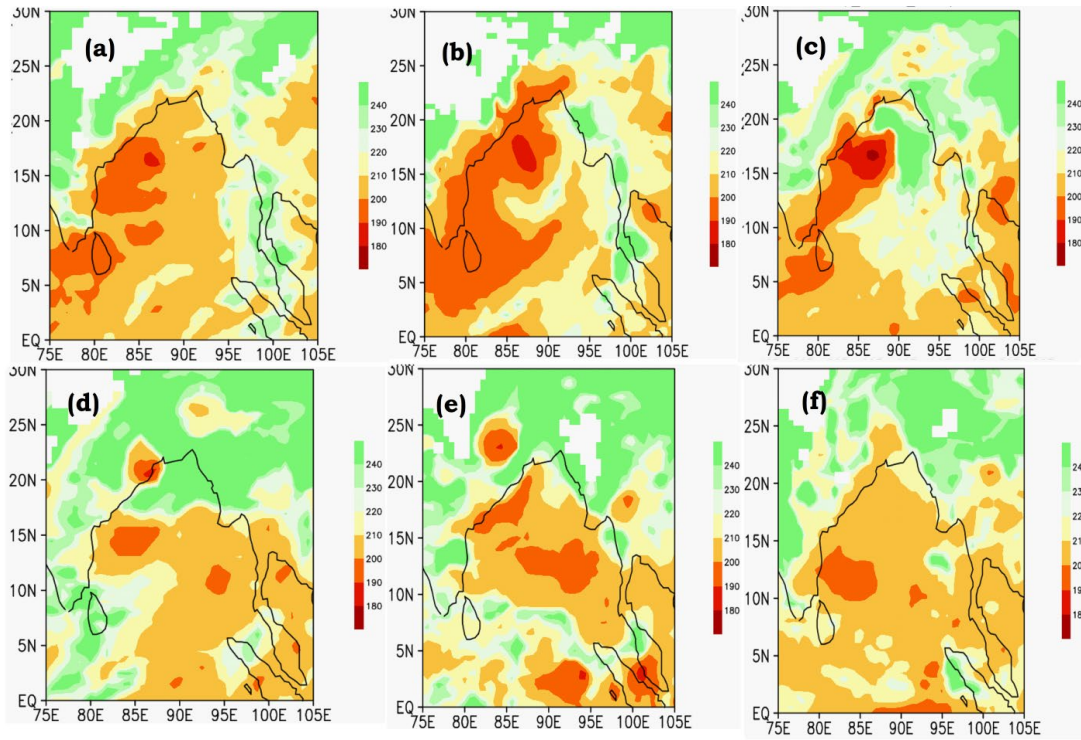


**Figure 2.** Spatial distribution of daily cloud top temperature during (a) May 23<sup>rd</sup>, 2021, (b) May 24<sup>th</sup>, 2021, (c) May 25<sup>th</sup>, 2021, (d) May 26<sup>th</sup>, 2021, (e) May 27<sup>th</sup>, 2021, (f) May 28<sup>th</sup>, 2021.

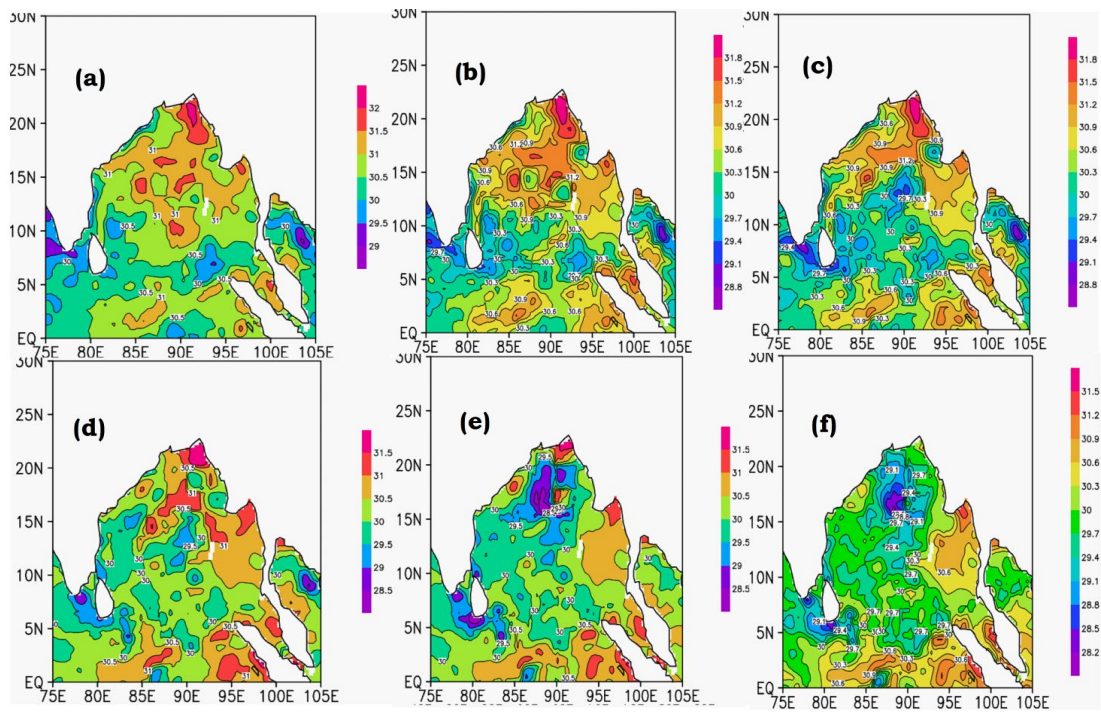


**Figure 3.** Spatial distribution of daily sea surface temperature during (a) May 23<sup>rd</sup>, 2021, (b) May 24<sup>th</sup>, 2021, (c) May 25<sup>th</sup>, 2021, (d) May 26<sup>th</sup>, 2021, (e) May 27<sup>th</sup>, 2021, (f) May 28<sup>th</sup>, 2021.

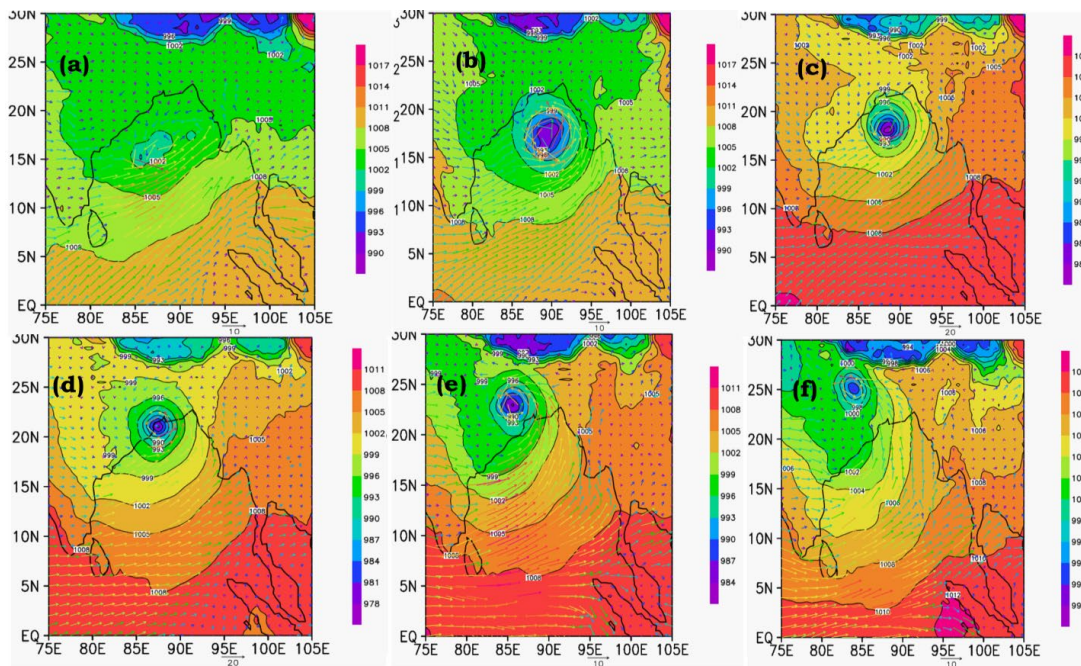


**Figure 4.** Daily sea level pressure distribution (in shaded areas) and wind vectors for the dates of (a) May 23, (b) May 24, (c) May 25, (d) May 26, (e) May 27, and (f) May 28 in 2021.

We have produced SLP (Shaded) and winds (Vectors) spatial maps across the BOBS region from May 23<sup>rd</sup> to May 28<sup>th</sup>, 2021 in Figure 4. On 23<sup>rd</sup> May, 2021, the SLP values are low near Central Andhra Pradesh coastal area in BOBS. The SLP values drops from 1002hpa to 999hpa over BOBS region. The wind vectors represent that the westerly winds are accumulated around the low pressure area and they move with a speed of nearly 10 m/s (Figure 4(a)). On 24<sup>th</sup> May, 2021, the SLP values are low near Northern Andhra Pradesh and Southern Odisha coastal area in BOBS. The SLP values drops from 1002hpa to 990hpa over BOBS region. Strong winds (10 m/s) have been seen close to the low pressure area, according to the wind vectors (Figure 4(b)). The SLP values are low near the beaches of Odisha in BOBS on May 25, 2021. Over the BOBS region, the SLP values decrease from 993 hpa to 981 hpa. According to the wind vectors (Figure 4(c)), strong wind gusts (20 m/s) have been seen near low pressure area. The SLP values are low around the Bahanaga coastal region of Odisha on May 26, 2021, according to BOBS. Over the BOBS region, the SLP values decrease from 990 hpa to 978 hpa. According to the wind vectors (Figure 4(d)), 20 m/s-per-second strong winds have been seen in the area surrounding the low pressure. The SLP values are low on May 27, 2021, around the coast of Odisha and in the BOBS land area. On May 26, the cyclone made landfall. Over the BOBS region, the SLP values decrease from 996 hpa to 984 hpa. According to the wind vectors (Figure 4(e)), 10 m/s-per-second gusty winds are seen in the area surrounding the low pressure. The SLP values are rising around the states of Odisha and Andhra Pradesh on May 28, 2021. On the 26<sup>th</sup>, the cyclone made landfall. As a result, over the BOBS region, the SLP values start rising on the 28<sup>th</sup>, from 1000hpa to 1008hpa. According to the wind vectors (Figure 4(f)), the wind speed has fallen to 10 m/s.

In Figure 5, we've presented TPW (Shaded) and divergence (Contour) spatial maps over the BOBS region from May 23<sup>rd</sup> to May 28<sup>th</sup>, 2021. The TPW values are high near the Central Andhra Pradesh coast in BOBS on May 23, 2021. Over the BOBS region, 50 to 70 mm is the range of the TPW values. The divergence values are in the range of -0.5 to -0.2, favoring the accumulation of moisture across the BOBS (Figure 5(a)). On 24<sup>th</sup> May, 2021, the TPW values are high near Northern Andhra Pradesh and Southern Odisha coastal areas in BOBS. Over the BOBS region, the TPW values range from 60 to 70 mm. The divergence values in BOBS (Figure 5(b)) range from -0.5 to -1.0, favouring moisture accumulation along the Odisha coast. The TPW values near the southern Odisha coast in BOBS are high on May 25, 2021. Over the BOBS region, TPW values range from 60 to 80 mm. The divergence values in BOBS (Figure 5(c)) ranges from -0.5 to -1.0, favouring moisture accumulation across the Odisha coastal areas. On 26<sup>th</sup> May, 2021, the TPW values are high near Bahanaga coast area near Odisha cast in BOBS. Over the BOBS region, the TPW values range from 60 to 80 mm. The divergence values in BOBS (Figure 5(d)) ranges from -0.1 to -0.3, favouring moisture accumulation along the Odisha beaches. On 27<sup>th</sup> May, 2021, the TPW values are high near Odisha coast and land area in BOBS. The TPW values lies between 55 and 65 mm over BOBS region. The divergence values range between -0.5 and -1.0 favouring the moisture accumulation across the Odisha coast (Figure 5(e)). On 28<sup>th</sup> May, 2021, the TPW values are high near Odisha area over land. The cyclone made landfall on 26<sup>th</sup>. So on 27<sup>th</sup>, the TPW values starts decreasing from 80 to 50 mm over Odisha region. The divergence values range between -0.1 and -0.3 across the BOBS (Figure 5(f)).

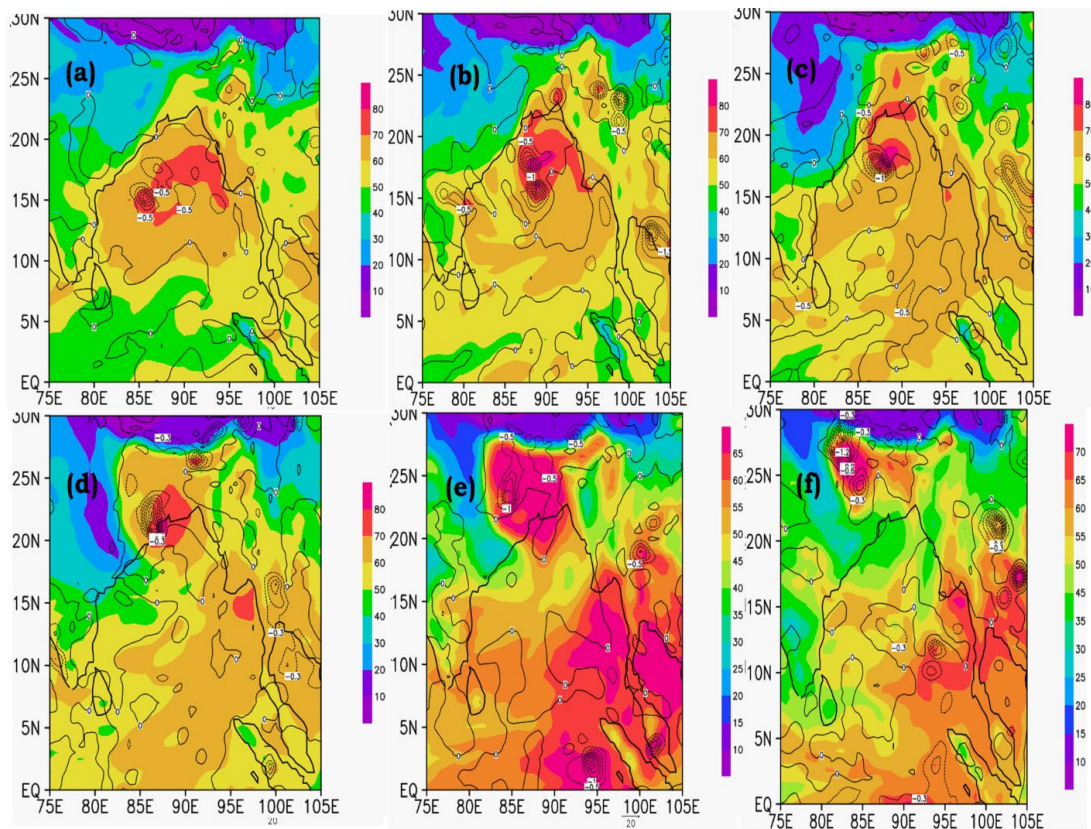


**Figure 5.** Spatial distribution of daily TPW (shaded) and divergence (contour) during (a) May 23<sup>rd</sup>, 2021, (b) May 24<sup>th</sup>, 2021, (c) May 25<sup>th</sup>, 2021, (d) May 26<sup>th</sup>, 2021, (e) May 27<sup>th</sup>, 2021, (f) May 28<sup>th</sup>, 2021.

We plotted CAPE spatial maps of the area surrounding the Bay of Bengal Sea between May 23 and May 28, 2021 (Figure 6). On May 23<sup>rd</sup>, 2021, CAPE levels in the BOBS region range from 1000 to 2000 J/kg (Figure 6(a)). On May 24<sup>th</sup>, 2021, CAPE levels in the BOBS region range from 1200 to 2100 J/kg (Figure 6(b)). The high CAPE is observed near Andhra Pradesh coastal areas on May 25<sup>th</sup>, 2021. Over BOBS, CAPE values range from 1500 to 2400 J/kg (Figure 6(c)). High CAPE values were observed around Odisha coastal areas on May 26<sup>th</sup>, 2021. Over BOBS, CAPE values vary from 1500 to 2700 J/kg (Figure 6(d)). The CAPE is greater near Odisha on May 27<sup>th</sup>, 2021. CAPE values over BOBS range from 1000 to 2500 J/kg (Figure 6(e)). On May 28, 2021, CAPE values along the coast of Odisha decreased over BOBS (Figure 6(f)). We produced spatial maps of LI over the Bay of Bengal Sea region from May 23 to May 28 of 2021 (Figure 7). On May 23<sup>rd</sup>, 2021, the LI values in the BOBS region range from -4 to -2 K (Figure 7(a)). On

the 24<sup>th</sup> of May, 2021, the LI values in the BOBS region vary from -4 to -2 K (Figure 7(b)). The low LI is visible near Andhra Pradesh coastal areas on May 25<sup>th</sup>, 2021. Over BOBS, LI values range from -6 to -4 K (Figure 7(c)). The LI values are seen around Northern Andhra Pradesh and Southern Odisha coastal areas on May 26<sup>th</sup>, 2021. Over BOBS, LI values vary from -6 to -4 K (Figure 7(d)). The LI values near Odisha ranged between -4 and -2 K on May 27<sup>th</sup>, 2021. Over BOBS, LI values vary from -2 to 0 K (Figure 7(e)). On the 28<sup>th</sup> of May, 2021, the LI values near the Odisha and Andhra Pradesh coasts plummeted over BOBS (Figure 7(f)). We have displayed geographical maps of CIN over the Bay of Bengal Sea region from May 23<sup>rd</sup> to May 28<sup>th</sup>, 2021 in Figure 8. CIN values in the BOBS region range between 100 and 300 J/kg from May 23<sup>rd</sup> to May 28<sup>th</sup>, 2021 (Figure 8(a-f)). This is a strong indicator of severe atmospheric instability.

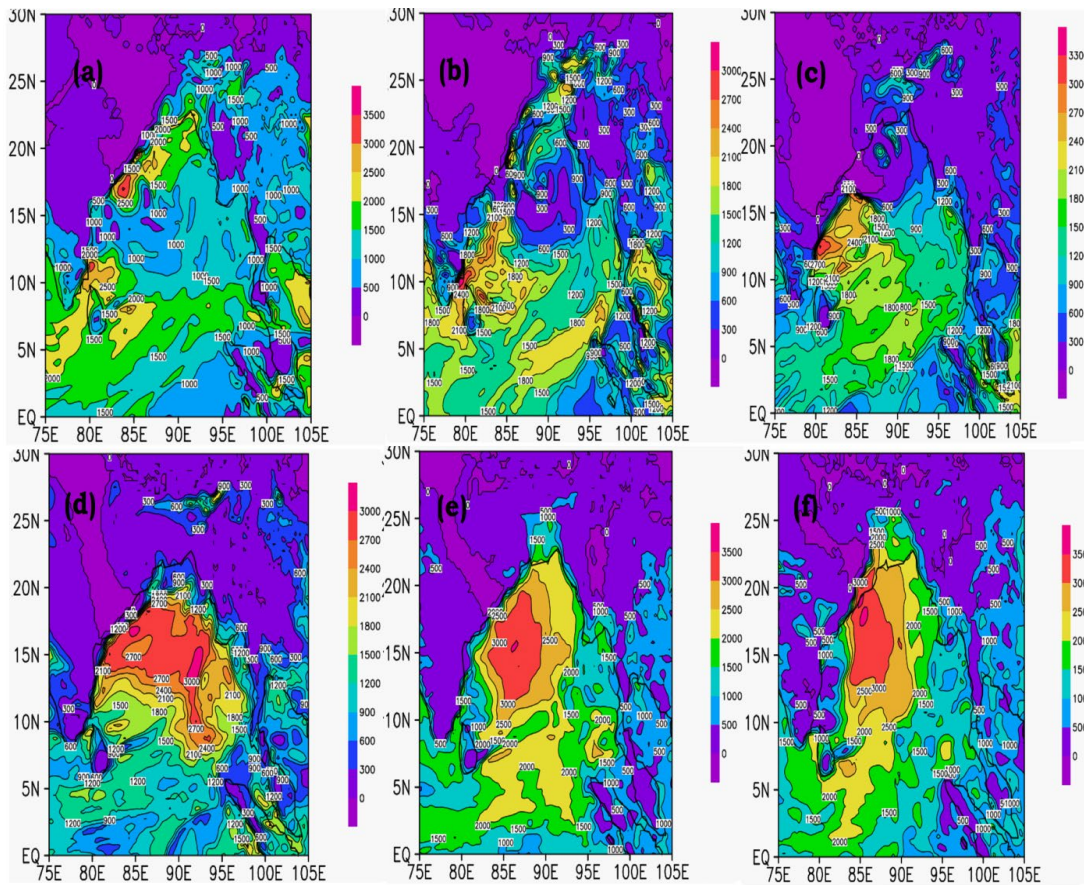


**Figure 6.** Spatial distribution of daily CAPE during (a) May 23<sup>rd</sup>, 2021, (b) May 24<sup>th</sup>, 2021, (c) May 25<sup>th</sup>, 2021, (d) May 26<sup>th</sup>, 2021, (e) May 27<sup>th</sup>, 2021, (f) May 28<sup>th</sup>, 2021.

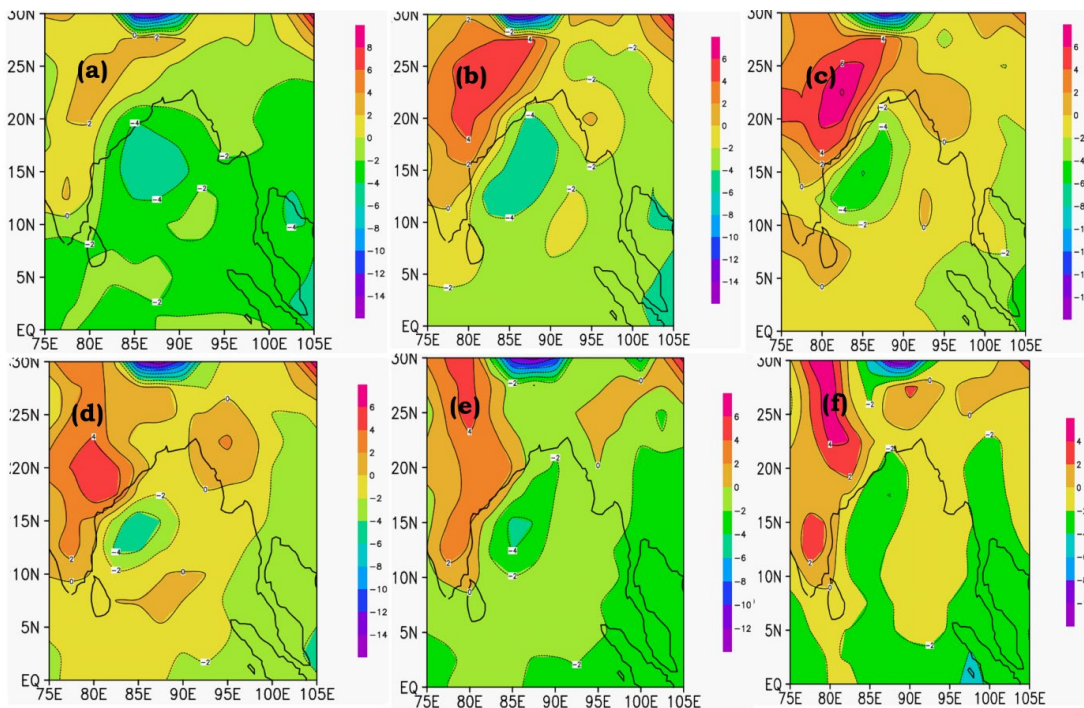


**Figure 7.** Spatial distribution of daily LI during (a) May 23<sup>rd</sup>, 2021, (b) May 24<sup>th</sup>, 2021, (c) May 25<sup>th</sup>, 2021, (d) May 26<sup>th</sup>, 2021, (e) May 27<sup>th</sup>, 2021, (f) May 28<sup>th</sup>, 2021.

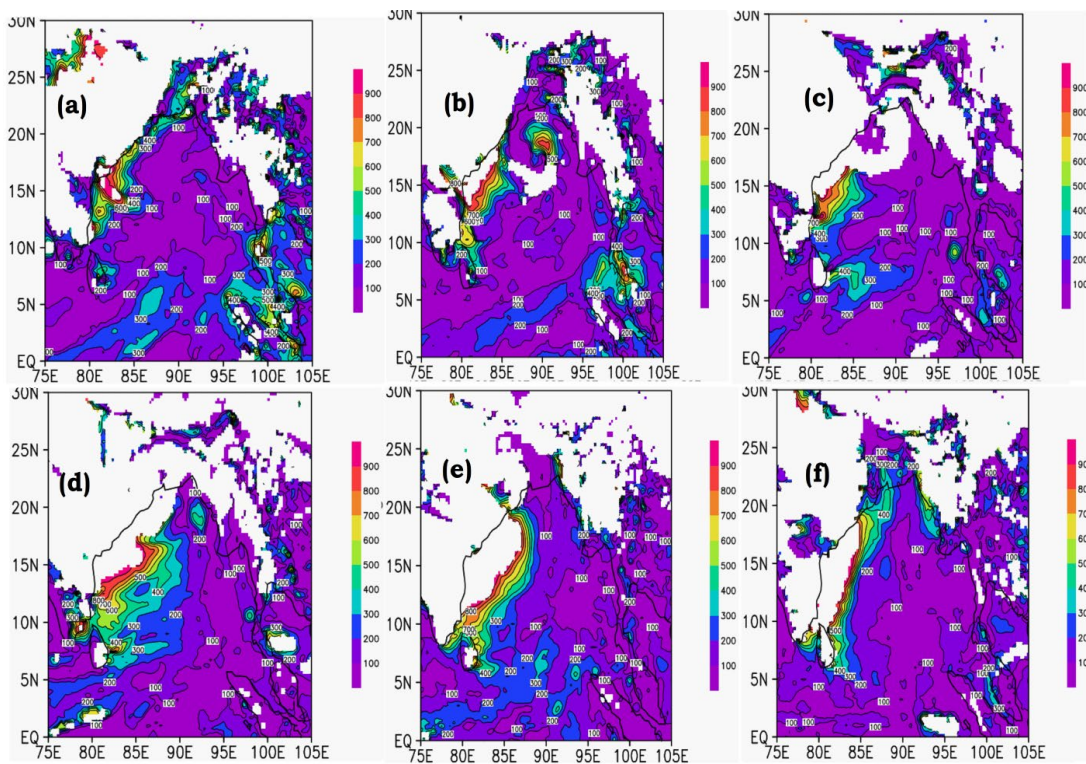


**Figure 8.** Spatial distribution of daily CIN during (a) May 23<sup>rd</sup>, 2021, (b) May 24<sup>th</sup>, 2021, (c) May 25<sup>th</sup>, 2021, (d) May 26<sup>th</sup>, 2021, (e) May 27<sup>th</sup>, 2021, (f) May 28<sup>th</sup>, 2021.

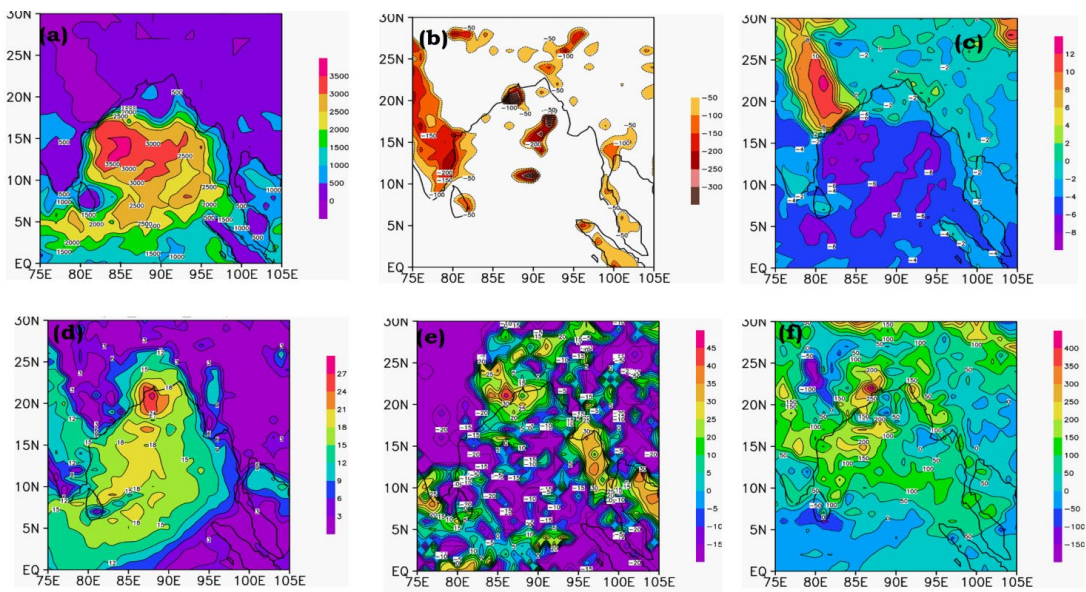


**Figure 9.** Spatial distribution of WRF calculated (a). CAPE parameter, (b). CIN parameter, (c). LI parameter, (d). wind gust parameter, (e). composite reflectivity parameter, (f). SRLH parameter, for May 26<sup>th</sup>, 2021.

**For Cyclone Yaas, the WRF Model Anticipated the Following Outcomes**

According to the IMD report, the cyclone made landfall on May 26, 2021, early in the morning (0330UTC). We have made an effort to forecast the cyclone Yaas prior using the WRF model. Since the storm reached landfall at 0330 UTC on May 26th, the WRF simulation started at 0000 UTC on May 22nd and ran throughout the full cyclonic event. The WRF model runs require six hours to spin up. High CAPE values were reported nearer the

North Andhra Pradesh coast and Southern Odisha coast on May 26<sup>th</sup>, 2021. The CAPE values nearly approached 3500 J/kg, indicating the seriousness of the situation (Figure 9). The CAPE anticipated by the WRF model was higher than the MERRA2 data. The WRF predicted CIN values also showed the convection severity of the cyclone. The values ranged between -50 and -200 which indicate severity near Dhamra port (Figure 10). The WRF predicted LI values ranged between -6 to -4 K at Orissa coast as seen in Figure 11. We have also tried to look at the wind gust in

WRF model. High wind gust is seen near north coast of Dhamra Port and south coastal area of Bahanaga. Wind gust values almost lie between 18 and 24 m/s indicating the severity of cyclone (Figure 12). The complex reflectivity values (~ 20 to 30) showed the severity of the cyclone occurrence prior (Figure 13). The SRLH values (~ 150 to 250) showed the severity of the cyclone occurrence prior (Figure 14). We can see that from Figure 9(a-f) the WRF predicted parameters almost indicated the severity of cyclone prior when compared to MERRA over BOBS.

#### 4. Summary and Conclusion

Between May 23 and May 28, 2021, a tropical cyclone named Yaas swept over the Bay of Bengal Sea. This study tries to better understand it. The discussion of the cyclone evolution tracked by instability indices provides a distinct perspective on the subject. It also makes it possible to analyze if these indices may be used to diagnose severe convection in situations of this nature. High rainfall was recorded along Odisha's coastal areas on May 26th, 2021. Over BOBS, rainfall ranges from 60 to 100 mm. CTT are significant because of their tight relationship to cloud top height (CTH). The lower is the CTT, the higher the cloud. As a result, the coldest IR pixels usually depict the highest tops of clouds, such as convective storm "overshooting tops." CTT is quite low around Odisha coastal area Bahanaga on May 26<sup>th</sup>, 2021. Over BOBS, CTT values range from 180 to 200K. A high rate of evaporation and moisture pumping into the cyclone can occur when the weather is sufficiently warm. Storms are made violent by the condensation of this vast volume of water vapor, which can result in massive amounts of rain when they impact land. High SST values were seen around Odisha coastal areas on May 26<sup>th</sup>, 2021. Over BOBS, SST values vary from 30.5 to 31.1°C. Intense tropical cyclones produce the lowest air pressure on the planet, when water vapor condenses to form clouds and rain, releasing heat that warms the air column in the storm's eye. The air rises around the low pressure, cools and condenses into clouds and precipitation as it does so. SLP values near the Odisha coastal area in BOBS are low on May 26<sup>th</sup>, 2021. Over the BOBS region, the SLP values drop from 990hpa to 978hpa. High winds of 20 m/s have been detected near the low pressure, according to the wind vectors. Divergence in the top layers of the atmosphere is required to keep the rising air currents within the cyclone pumped out and the cyclone's core pressure low. There is a region of divergence aloft above the developing low-pressure centre if the upper levels are conducive for cyclone development. This will aid in the upward movement of air that is converging at the surface and the development of the surface cyclone. The TPW values around Bahanaga coastal area of Odisha coast in BOBS are high on the 26<sup>th</sup> of May, 2021. Over the BOBS region, the TPW values vary from 60 to 80 mm. The divergence values in BOBS range from -0.1 to -0.3, favoring moisture accumulation along the coastal areas of Odisha. High CAPE values were observed around Odisha coastal areas on May 26<sup>th</sup>, 2021. CAPE values across BOBS range from 1000 to 3500 J/kg. A stability metric that can be used to gauge the atmosphere's buoyancy is the lifted index. As one increases altitude, the temperature of the atmosphere decreases. Air cools as it ascends

to the surface. Occasionally, nevertheless, it does cool more slowly than its surroundings.) On May 26, 2021, coastal parts of Odisha have extremely low LI values. LI values over BOBS range from -4 to -2 K. When compared to MERRA over BOBS, WRF predicted metrics almost indicated the strength of the cyclone previously.

#### 5. Acknowledgements

Authors thank the European Centre for Medium Range Weather Forecasting (ECMWF) for providing a free accessible dataset of Copernicus Climate Change Service (C3S) for our study. We also thank National Aeronautics and Space Administration (NASA) for providing free available datasets of MERRA and GPM IMERG for this analysis.

#### 6. References

- Balaguru, K., Chang, P., Saravanan, R., Leung, L. R., Xu, Z., Li, M., & Hsieh, J. S (2012) Ocean barrier layers' effect on tropical cyclone intensification. *Proceedings of the National Academy of Sciences*, 109(36), 14343-14347.
- Das Someshwar., Ashrit, R., Moncrieff, M.W (2006a) Simulation of a Himalayan Cloudburst Event. *Journal of Earth System Science*, 115(3), 299-313.
- Carlson, T. N., Perry, E. M., & Schmutge, T. J (1990) Remote estimation of soil moisture availability and fractional vegetation cover for agricultural fields. *Agricultural and Forest Meteorology*, 52(1-2), 45-69.
- Chowdhury, A. M. R., Bhuyia, A. U., Choudhury, A. Y., & Sen, R (1993) The Bangladesh cyclone of 1991: why so many people died. *Disasters*, 17(4), 291-304.
- Conte, D., Miglietta, M. M., and Levizzani, V (2011) Analysis of instability indices during the development of a Mediterranean tropical-like cyclone using MSG-SEVIRI products and the LAPS model. *Atmospheric research*, 101(1-2), pp. 264-279.
- Dasgupta, S., Huq, M., Khan, Z. H., Ahmed, M. M. Z., Mukherjee, N., Khan, M., & Pandey, K. D (2010) Vulnerability of Bangladesh to cyclones in a changing climate: Potential damages and adaptation cost. *World Bank Policy Research Working Paper*, (5280).
- DeMaria, M (1996) The effect of vertical shear on tropical cyclone intensity change. *Journal of Atmospheric Sciences*, 53(14), 2076-2088.
- Dudhia, J (1989) Numerical study of convection observed during the winter monsoon experiment using a mesoscale two dimensional model. *J. Atmos. Sci.* 46, 3077-3107, doi: 10.1175/1520-0469(1989)046<3077: NSOCOD>2.0.CO; 2.

- Galway, J. G (1956) The lifted index as a predictor of latent instability. *Bulletin of the American Meteorological Society*, 37(10), 528-529.
- Gelaro, R., McCarty, W., Suárez, M. J., Todling, R., Molod, A., Takacs, L., & Zhao, B (2017) The modern-era retrospective analysis for research and applications, version 2 (MERRA-2). *Journal of climate*, 30(14), 5419-5454.
- Gray, W. M (1968) Global view of the origin of tropical disturbances and storms. *Monthly Weather Review*, 96(10), 669-700.
- Gray, W. M (1975) Tropical cyclone genesis (Doctoral dissertation, Colorado State University. Libraries).
- Gray, W. M (1998) The formation of tropical cyclones. *Meteorology and atmospheric physics*, 67(1), 37-69.
- Hersbach, H., Bell, B., Berrisford, P., Hirahara, S., Horányi, A., Muñoz-Sabater, J., & Thépaut, J. N (2020) The ERA5 global reanalysis. *Quarterly Journal of the Royal Meteorological Society*, 146(730), 1999-2049.
- Hossain, I., & Mullick, A. R (2020) Cyclone and Bangladesh: A historical and environmental overview from 1582 to 2020. *International Medical Journal*, 25(6), 2595-2614.
- Hossain, M. Z., Islam, M. T., Sakai, T., & Ishida, M (2008) Impact of tropical cyclones on rural infrastructures in Bangladesh. *Agricultural Engineering International: CIGR Journal*.
- Huffman, G. J., Stocker, E. F., Bolvin, D. T., Nelkin, E. J., Jackson, Tan (2019) GPM IMERG Early Precipitation L3 Half Hourly 0.1 degree x 0.1 degree V06, Greenbelt, MD, Goddard Earth Sciences Data and Information Services Center (GES DISC), Accessed: [Data Access Date], 10.5067/GPM/IMERG/3B-HH-E/06
- Islam, M. T., Hossain, M. Z., & Ishida, M (2011) Trends analyses for several factors affected by tropical cyclones. *American Journal of Environmental Sciences*, 7(3), 200-206.
- Islam, T., & Peterson, R. E (2009) Climatology of landfalling tropical cyclones in Bangladesh 1877–2003. *Natural Hazards*, 48(1), 115-135.
- Karim, M. F., & Mimura, N (2008) Impacts of climate change and sea-level rise on cyclonic storm surge floods in Bangladesh. *Global environmental change*, 18(3), 490-500.
- Karyampudi, V. M., & Pierce, H. F (2002) Synoptic-scale influence of the Saharan air layer on tropical cyclogenesis over the eastern Atlantic. *Monthly weather review*, 130(12), 3100-3128.
- Koenig, M., & De Coning, E (2009) The MSG global instability indices product and its use as a nowcasting tool. *Weather and forecasting*, 24(1), 272-285.
- König, M., Tjemkes, S., & Kerkmann, J (2002) Atmospheric instability parameters derived from MSG SEVIRI observations. Darmstadt, Germany: EUMETSAT.
- Le Marshall, J. F., & Riley, P (1994) Real-time assimilation and synoptic application of local TOVS raw radiance observations. *Australian Meteorological Magazine*, 43(3), 153-166.
- Ma, X. L., Schmit, T. J., & Smith, W. L (1999) A nonlinear physical retrieval algorithm—its application to the GOES-8/9 sounder. *Journal of Applied Meteorology*, 38(5), 501-513.
- Maloney, E. D., Gettelman, A., Ming, Y., Neelin, J. D., Barrie, D., Mariotti, A., & Zhao, M (2019) Process-oriented evaluation of climate and weather forecasting models. *Bulletin of the American Meteorological Society*, 100(9), 1665-1686.
- Maloney, E. D., & Hartmann, D. L (2000) Modulation of eastern North Pacific hurricanes by the Madden-Julian oscillation. *Journal of climate*, 13(9), 1451-1460.
- Maloney, E. D., & Hartmann, D. L (2000) Modulation of hurricane activity in the Gulf of Mexico by the Madden-Julian oscillation. *Science*, 287(5460), 2002-2004.
- Mazzarella, L. A., Ritchie, E. A., & Wood, K. M (2014) 2C. 7 EASTERN NORTH PACIFIC TROPICAL CYCLOGENESIS USING SATELLITE-BASED OBSERVATIONS.
- Mcphaden, M. J., Foltz, G. R., Lee, T., Murty, V. S. N., Ravichandran, M., Vecchi, G. A., & Yu, L (2009) Ocean-atmosphere interactions during cyclone nargis. *EOS, Transactions American Geophysical Union*, 90(7), 53-54.
- Mecikalski, J. R., Mackenzie Jr, W. M., & Bedka, K. M (2008) Algorithm for convective initiation for GOES-R. NOAA NESDIS Algorithm Theoretical Basis Document, 30pp.
- Mecikalski, J. R., Feltz, W. F., Murray, J. J., Johnson, D. B., Bedka, K. M., Bedka, S. T., & Williams, E (2007) Aviation applications for satellite-based observations of cloud properties, convection initiation, in-flight icing, turbulence, and volcanic ash. *Bulletin of the American Meteorological Society*, 88(10), 1589-1607.
- Menzel, W. P., Holt, F. C., Schmit, T. J., Aune, R. M., Schreiner, A. J., Wade, G. S., & Gray, D. G (1998) Application of GOES-8/9 soundings to weather forecasting and nowcasting. *Bulletin of the American Meteorological Society*, 79(10), 2059-2078.
- Mlawer, E. J., Taubman, S. J., Brown, P. D., Iacono, M. J., Clough, S. A (1997) Radiative transfer for inhomogeneous atmosphere:

- RRTM, a validated correlated-k model for the long-wave. *J. Geophys. Res.* 102, 16663–16682, doi: 10.1029/97JD00237.
- Moncrieff, M. W., & Miller, M. J (1976) The dynamics and simulation of tropical cumulonimbus and squall lines. *Quarterly Journal of the Royal Meteorological Society*, 102(432), 373-394.
- Morrison, H., Curry, J. A., Shupe, M. D., Zuidema, P (2005) A new double-moment microphysics parameterization for application in cloud and climate models. Part II: Single-column modeling of arctic clouds. *J. Atmos. Sci.* 62, 1678–1693.
- Moscattello, A., Marcello Miglietta, M., & Rotunno, R (2008) Observational analysis of a Mediterranean hurricane over south-eastern Italy. *Weather*, 63(10), 306.
- Parker, D. J (2002) The response of CAPE and CIN to tropospheric thermal variations. *Quarterly Journal of the Royal Meteorological Society: A journal of the atmospheric sciences, applied meteorology and physical oceanography*, 128(579), 119-130.
- O'Hare, G (2001) Hurricane 07B in the Godavari Delta, Andhra Pradesh, India: vulnerability, mitigation and the spatial impact. *Geographical Journal*, 167(1), 23-38.
- Purdum, J. F (1976) Some uses of high-resolution GOES imagery in the mesoscale forecasting of convection and its behavior. *Monthly Weather Review*, 104(12), 1474-1483.
- Rajeevan, M., Kesarkar, A., Thampi, S.B., Rao, T. N., Radhakrishna, B., Rajasekhar, M (2010) Sensitivity of WRF cloud microphysics to simulations of a severe thunderstorm event over Southeast India. *Ann. Geophysic.*, 28, 603–619.
- Roberts, R. D., & Rutledge, S (2003) Nowcasting storm initiation and growth using GOES-8 and WSR-88D data. *Weather and Forecasting*, 18(4), 562-584.
- Scoccimarro, E., Fogli, P. G., Reed, K. A., Gualdi, S., Masina, S., & Navarra, A (2017) Tropical cyclone interaction with the ocean: The role of high-frequency (subdaily) coupled processes. *Journal of Climate*, 30(1), 145-162.
- Seemann, S. W., Li, J., Menzel, W. P., & Gumley, L. E (2003) Operational retrieval of atmospheric temperature, moisture, and ozone from MODIS infrared radiances. *Journal of Applied Meteorology and Climatology*, 42(8), 1072-1091.
- Siddique, A. K., & Eusof, A (1987) Cyclone deaths in Bangladesh, May 1985: who was at risk. *Tropical and geographical medicine*, 39(1), 3-8.
- Siewert, C. W., Koenig, M., & Mecikalski, J. R (2010) Application of Meteosat second generation data towards improving the nowcasting of convective initiation. *Meteorological Applications*, 17(4), 442-451.
- Singh, O. P (2007) Long-term trends in the frequency of severe cyclones of Bay of Bengal: observations and simulations. *Mausam*, 58(1), 59-66.
- Skamarock WC, Klemp J, Dudhia J, Gill DO, Barker DM, Wang W and Powers JG 2005 A Description of the Advanced Research WRF Version 2. NCAR Technical Note; NCAR/TN-468+STR. Mesoscale and Microscale Meteorology Division, National Center for Atmospheric Research, Boulder, Colorado, USA.
- Skamarock, W. C., Klemp, J. B., Dudhia, J., Gill, D. O., Zhiquan, L., Berner, J., Wang, W., Powers, J.G., Duda, M.G., Barker, D.M., Huang, X. Y (2019) A Description of the Advanced Research WRF Model Version 4. NCAR Tech. Note NCAR/TN-475+STR 145. <https://doi.org/10.5065/1dfh-6p97>.
- Smith, W. P., & Gall, R. L (1989) Tropical squall lines of the Arizona monsoon. *Monthly weather review*, 117(7), 1553-1569.
- Sriver, R., & Huber, M (2006) Low frequency variability in globally integrated tropical cyclone power dissipation. *Geophysical Research Letters*, 33(11).
- Sreenivas, P., & Gnanaseelan, C (2013) Impact of oceanic processes on the life cycle of severe cyclonic storm "Jal". *IEEE Geoscience and Remote Sensing Letters*, 11(2), 519-523.
- Sreenivas, P., Gnanaseelan, C., & Prasad, K. V. S. R (2012a) Influence of El Niño and Indian Ocean Dipole on sea level variability in the Bay of Bengal. *Global and Planetary Change*, 80, 215-225.
- Sreenivas, P., Chowdary, J. S., & Gnanaseelan, C (2012b) Impact of tropical cyclones on the intensity and phase propagation of fall Wyrтки jets. *Geophysical research letters*, 39(22).
- Sun, D., Kafatos, M., Cervone, G., Boybeyi, Z., & Yang, R (2007) Satellite microwave detected SST anomalies and hurricane intensification. *Natural Hazards*, 43(2), 273-284.
- Velasco, I., Fritsch, J.M (1987) Mesoscale convective complexes in the Americas; *Geophys Res* 92 9591–9613.
- Venkatesh, T. N (2006) Mesoscale interactions during the genesis and intensification of October 1999 Orissa super cyclone. *Mausam*, 57(1), 31-36.
- Webster, P. J (2008) Myanmar's deadly daffodil. *Nature Geoscience*, 1(8), 488-490.
- Wu, L., Su, H., Fovell, R. G., Wang, B., Shen, J. T., Kahn, B. H., & Jiang, J. H (2012) Relationship of environmental relative

humidity with North Atlantic tropical cyclone intensity and intensification rate. *Geophysical research letters*, 39(20).

Zehnder, J. A., & Gall, R. L (1991) Alternative mechanisms of tropical cyclone formation in the Eastern North Pacific. *Atmósfera*, 4(1), 37-51.

Zehr, R. M (2003) Environmental vertical wind shear with Hurricane Bertha (1996). *Weather and forecasting*, 18(2), 345-356.